Chapter 8

Mitochondrial Trafficking by Prohibitin-Kinesin-Myosin-Cadherin Complex in the Eye

Srinivas R. Sripathi, Weilue He, Johnpaul Offor,
Diana R. Gutsaeva and Wan Jin Jahng

Additional information is available at the end of the chapter

http://dx.doi.org/10.5772/intechopen.75994

Abstract

Disruption of the mitochondrial-nuclear network leads to accelerated aging and age-related diseases, including age-related macular degeneration. The current study tested the hypothesis that mitochondrial morphology could be demonstrated quantitatively using a mathematic model and mitochondrial trafficking complex under stress conditions. To test our hypothesis, normal and aberrant mitochondria were examined quantitatively based on mitochondrial size, shape, position, composition, and dynamics. Adaptation of the mitochondrial network to changes in the intracellular oxidation and reduction milieu is critical for the survival of retinal pigment epithelial cells. Our mitochondrial interactome mapping demonstrated that a positive correlation may exist between oxidative stress-mediated phosphorylation and age-related disease progression. The current interactome may provide a potential therapeutic approach to treat mitochondria-induced neurodegeneration, including age-related macular degeneration.

Keywords: mitochondrial trafficking, prohibitin-cytoskeleton, retinal pigment epithelial cells, mitochondrial dynamics, age-related macular degeneration, protein interactome

1. Introduction

Mitochondria are the highly dynamic cellular organelles that form a dynamic network to regulate calcium balance, energy metabolism, and apoptotic signaling [1–8]. Mitochondria alter their morphology repeatedly through the collective actions of fission as a separation of a single organelle into multiple autonomous structures, fusion as the combination of multiple

structures to form single organelle, as well as movement along cytoskeletal paths [5, 9]. These combined actions occur concurrently in major cell types to regulate the cell fate.

To maintain the balance that regulates overall morphology and cytoskeletal stability many specialized molecules including dynamin family of proteins play critical roles [10, 11]. Growing body of evidence demonstrates that disruptions of mitochondrial network lead to multiple human pathologies, including metabolic, genetic, cardiovascular diseases, as well as neurogenerative diseases and cancers [12–15]. Several studies provided the evidence that mitochondria play a critical role in the progression of age-related diseases, including age-related macular degeneration (AMD) [16–21]. The damage of mitochondrial DNA could be the key factor involved in altered vascular endothelial growth factor (VEGF) secretion, retinal pigment epithelium (RPE) dysfunction, and cell death during the progression of AMD [22, 23].

The current study aimed to examine the correlation between alterations in mitochondrial morphology and mitochondrial dysfunction. For quantitative analysis of mitochondrial morphology, we introduced the mitochondrial index that includes network size, mitochondrial content and surface area. Mitochondrial interconnectivity and elongation were determined systematically using a computational model in three dimensions, showing a mitochondrial-endoplasmic reticulum (ER)-nuclear hole as open space for trafficking at the beginning of apoptosis under oxidative stress.

The assessment of average circularity showed mitochondrial elongation which is sensitive to fragmented vs. normal shaped mitochondria. The average area/perimeter ratio showed normal or stressed mitochondria as a highly interconnected mass of reticular network. Previously, we observed that prohibitin translocalizes between the nucleus and mitochondria under oxidative stress conditions to influence mitochondrial dynamics [24]. We observed anterograde signaling from the nucleus to mitochondria using a prohibitin shuttle under stress in the retina, as well as the retrograde shuttling of prohibitin from mitochondria to the nucleus in the RPE. In addition, cytoskeletal reorganization, tubulin/vimentin depolymerization and increased phosphorylations were observed in stressed mitochondria [25–27].

In this study, mitochondrial dynamics was further analyzed in mitochondrial trafficking complex using prohibitin immunoprecipitation. We found a motor-based protein complex that includes kinesin 19 (93 kDa), myosin 9 (110 kDa), and cadherin isoforms (88 kDa) to regulate the mitochondrial-nuclear communication. Finally, we have established a comprehensive mitochondrial interactome map by combining several independent sets of interaction data. Our interactome map provides an integrated information on the hidden apoptotic pathway, cytoskeletal rearrangement, nitric oxide signaling, ubiquitination, and mitochondrial network in neurodegeneration.

2. Materials and methods

2.1. Cell culture and oxidative stress treatment

Retinal pigment epithelial cells (ARPE-19) were purchased from ATCC (Manassas, VA) and cultured in Dulbecco's modified Eagle's medium (DMEM) supplemented with fetal bovine

serum (FBS; 10%) and penicillin/streptomycin (1%) at 37°C in a humidified atmosphere of 5% CO_2 in air as suggested by the manufacturer. Cells were used between passages 8–9.

Retinal progenitor cells (HRP) were kindly donated by Dr. Harold J. Sheeldo (University of North Texas Health Science Center) and were cultured at the same condition as ARPE-19 cells.

Prior to all experiments, confluent ARPE-19 cells were incubated with fresh medium for 12 h and washed with phosphate buffered saline (PBS) three times. ARPE-19 cells were incubated with an oxidant, *tert*-butyl hydroperoxide (*t*-BuOOH, 200 μM, Sigma-Aldrich, St.Louis, MO), in serum-free medium for 0.5, 1, 2, 4, 6, 8, 12, and 24 h and representative images were presented. After the treatment, medium was removed, cells were washed with PBS and harvested for future analysis. Cells were lysed for experiments, including, immunoprecipitation, sodium dodecyl sulfate polyacrylamide gel electrophoresis (SDS–PAGE), Western blot analysis, immunocytochemistry, and mass spectrometry analysis.

To compare with other stress environment, ARPE-19 cells were incubated under intense light (210 μmoles/m^2/s photon flux; 7000 lx) for 1 h in serum-free media and analyzed by SDS-PAGE/Western blotting, or immunocytochemistry.

Lipids were extracted from ARPE-19 cells using cholorform/methanol (2:1, v/v) and organic solvent was evaporated under a gentle nitrogen stream and dissolved in chloroform for analysis by HPLC and mass spectrometry.

All experiments were repeated (N = 3–10 biological samples) with technical duplicate or triplicate. Statistical analysis was performed using StatView software and statistical significance was determined by variance (ANOVA) or unpaired Student's t test when appropriate.

2.2. Donor eye tissue and phosphoprotein enrichment

Human postmortem donor eye tissues were used following the tenets of the Declaration of Helsinki. Human AMD retinas (8 mm macular and peripheral punches), RPE (8 mm central and peripheral punches), and age-matched control eyes (N = 9, biological triplicate x technical triplicate) were provided by the Lions Eye Bank (Moran Eye Center, University of Utah). Phosphoproteome of macular (I), peripheral retina (II), central RPE (III), and peripheral RPE (IV) was compared to age-matched control donor eyes to determine region-specific senescence-associated molecular mechanisms during AMD progression. Phosphoproteins were enriched by charge-based spin column chromatography and resolved by 2D gel electrophoresis as previously reported [28]. In addition, trypsin digested phosphopeptides from whole lysates were enriched using Ga^{3+}/TiO_2 immobilized metal ion chromatography. Eluted phosphopeptides were analyzed using mass spectrometry including MALDI-TOF-TOF and ESI MS/MS.

2.3. Immunocytochemical analysis

To analyze mitochondrial morphology, Cells were incubated with 100 nM MitoTracker Orange (Molecular Probes). Cells were fixed using 10% formaldehyde (25 min) and the membrane was permeabilized using 0.2% Triton X-100 (20 min), followed by blocking (0.05% Tween 20, 10% FBS, 1 h) and incubation overnight at 4°C with anti-prohibitin antibody

(1:500; Genemed Synthesis, San Antonio). Prohibitin was visualized using Alexa Fluor 488-secondary IgG antibody (1:700; 1 h at 25°C; Molecular Probes). The nuclei were visualized by incubation with DAPI (4, 6-diamidino-2-phenylindole) added to VECTASHIELD Mounting Medium (Vector Laboratories, Burlingame, CA). A fluorescence microscopy was used for image analysis (Zeiss AxioVert 200 M Apo Tome, 63×).

2.4. Immunoprecipitation

ARPE-19 cells were rinsed (Modified Dulbecco's PBS) and lysed using immunoprecipitation (IP) lysis buffer (pH 7.4) containing Tris (25 mM), NaCl (150 mM), EDTA (1 mM), NP-40 (1%), glycerol glycerol (5%), and protease inhibitor cocktail by incubating on ice for 5 min with periodic sonication (3 × 5 min), followed by centrifugation (13,000 × *g*, 10 min). Proteins (1 mg/mL, 200–400 μL) were loaded for immunoprecipitation and nonspecific bindings were avoided using control agarose resin cross-linked by 4% bead agarose. Amino-linked protein-A beads were used to immobilize anti-prohibitin antibody with a coupling buffer (1 mM sodium phosphate, 150 mM NaCl, pH 7.2), followed by incubation (room temperature, 2 h) with sodium cyanoborohydride (3 μL, 5 M). Columns were washed using a washing buffer (1 M NaCl), and protein lysate was incubated in the protein A-antibody column with gentle rocking overnight at 4°C. The unbound proteins were spun down as flow-through, and the column was washed three times using the washing buffer (1 M NaCl) to remove nonspecific binding proteins. The prohibitin-interacting proteins were eluted by incubating with elution buffer for 5 min at room temperature. The eluted proteins were equilibrated with Laemmli sample buffer (5X, 5% β-mercaptoethanol). Eluted proteins were separated using SDS–PAGE and visualized using Coomassie blue (Pierce, IL) or silver staining kit (Bio-Rad, Hercules, CA). Prohibitin and p53 were visualized using Western blot analysis. Proteins were identified by mass spectrometry analysis.

2.5. Mass spectrometry analysis

Protein bands were excised into 1 × 1 × 1 mm cubes. The Coomassie-stained or silver-stained gel pieces were incubated using a Coomassie destaining buffer (200 μL of 50% MeCN in 25 mM NH_4HCO_3, pH 8.0, room temperature, 20 min) or silver destaining buffer (50% of 30 mM potassium ferricyanide, 50% of 100 mM sodium thiosulfate, 5–10 min). The gel pieces were dehydrated (200 μL, MeCN) and vacuum-dried (Speed Vac, Savant, Holbrook, NY). Proteins were reduced (10 mM DTT, 100 mM NH_4HCO_3, 30 min, 56°C) and were alkylated (55 mM iodoacetamide, 100 mM NH_4HCO_3, 20 min, room temperature in the dark). Proteins were digested using trypsin (13 ng/μL sequencing-grade from Promega, 37°C, overnight) in NH_4HCO_3 (10 mM) containing MeCN (10%). The peptides were enriched using a buffer (50 μL, 50% MeCN in NH_4HCO_3, 5% formic acid, 20 min, 37°C). Dried peptides were dissolved in the mass spectrometry sample buffer (5–10 μL, 75% MeCN in NH_4HCO_3,1% trifluoroacetic acid). Alpha-cyano-4-hydroxycinnamic acid (5 mg/mL, Sigma-Aldrich, St. Louis, MO) was freshly dissolved in a matrix buffer (50% MeCN, 50% NH_4HCO_3, 1% triflouroacetic acid) and centrifuged (13,000× *g*, 5 min). The peptide-matrix mixtures (0.5 μL) were spotted onto the MALDI target plate (Ground steel, Bruker Daltonics, Germany). Mass spectrometer and all

spectra were calibrated using a known peptide, including trypsin (842.5099, 2211.105 Da). The mass spectrum was recorded in 800–3000 Da range using Flex MALDI-TOF mass spectrometer (Bruker Daltonics, Germany, 70–75% laser intensity, 100–300 shots). Mass spectrometry data were analyzed using Flex analysis software (Bruker Dal- tonics, Germany). Peptides were identified using the Mascot software (Matrix Science) and NCBI/SwissProt database (zero mismatch cleavage, carbamidomethyl cysteine, methionine oxidation, 50–300 ppm mass tolerance). Peptide identification was evaluated based on Mascot MOWSE score, number of matched peptides, and protein sequence coverage. MOWSE score is expressed as -10logP as a probability value to compute the composite probability P.

2.6. Quantitative analysis of mitochondrial morphology

The connectivity, the number of mitochondrial branch points, and the interactive 3D visualization of isosurfaces were examined to identify the contact area between mitochondria and other organelles.

Mitochondria were stained using MitoTracker Orange/Red or rhodamine 123. Mitochondrial interconnectivity and elongation were analyzed systematically using computational software, including Mito-Morphology macro, Mitograph 2.0, Imaris 8.2.1., and SOAX 3.6.1.

Mitochondrial size and morphology were analyzed using the software connected to Image J software (Ruben Dagda: http://imagejdocu.tudor.lu/doku.php?id=macro:mitpophagy_ mitochondrial_morphology_content_lc3_colocalization_macro). We chose the region of interest using the polygon selection tool to analyze mitochondrial morphology. Individual red, green, and blue channels were obtained from the RGB images, and then the red and blue channels were closed. The grayscale was extracted from the red channel and the pixels were inverted to photographic channel. The Threshold function determined maximal and minimal pixel values. To understand mitochondrial structure and function, 12 mitochondrial indexes, including (1) mitochondrial area, (2) cellular area, (3) mitochondrial content, (4) perimeter, (5) circularity, (6) average perimeter, (7) average mitochondrial area, (8) average circularity, (9) area/perimeter, (10) area/perimeter normalized to minor axis, (11) minor axis, (12) area/perimeter normalized to circularity, were evaluated in ARPE-19 cells under oxidative stress conditions.

Mitochondrial shape, including fused, fragmented, tubular, swollen, branched, uniform, and perinuclear clustering, was examined quantitatively. Mitochondrial filaments in three dimensions and mitochondrial parameters in ARPE-19 cells were calculated mathematically using Image J and Imaris (v8.2.1) software. The connectivity, the number of mitochondrial branch points, and the interactive 3D visualization of isosurfaces were examined to identify the contact between mitochondria and other organelles.

2.7. Mitochondrial mapping in AMD

Mitochondrial signaling in a network-based interactome map between genome, proteome, and metabolome of AMD was established using proteome data and bioinformatics software. The protein-protein interaction was established using the Münich Information Center for Protein Sequence (MIPS), Biomolecular Interaction Network Database (BIND), the Database of

Interacting Proteins (DIP), the Molecular Interaction Database (MINT), the Protein Interaction Database (IntAct), and STRING.

Interaction mapping of prohibitin was determined using immunoprecipitation, followed by mass spectrometry analysis. Prohibitin binding proteins in the RPE were connected using STRING 10.0 software (http://string-db.org/).

Prohibitin interactions were confirmed using eight sources that include neighborhood, gene fusion, co-occurence, high-throughput interaction experiments, databases, homology, conserved co-expression, and published knowledge, including ExPASy (http://www.expasy.org/proteomics /protein–protein_interaction), MIPS (http://mips.helmholtz-muenchen.de/proj/ppi/), and Pubmed database (http://www.ncbi.nlm.nih.gov/pubmed).

AMD and oxidative biomarkers interactome were established using protein–protein interaction map software and databases, including STRING 10.0 (http://string-db.org/), MIPS and iHOP (http://www.ihop-net.org/UniPub/iHOP/) (**Figure 8**). Proteins found in AMD or oxidative stress conditions were added to establish the AMD interactome. Protein interactions were presented using eight categories, including neighborhood (green), gene fusion (red), co-occurrence (dark blue), co-expression (black), binding experiments (purple), databases (blue), text mining (lime), and homology (cyan). Protein interactions were determined and confirmed by genomic context, high-throughput experiments, co-expression, and previous publications in Pubmed. Protein database analysis showed the region-specific phosphorylation of specific proteins in AMD eyes. The interactome between AMD proteome was compared to the retina/RPE proteome under stress conditions.

The genome regulatory network was connected to the proteome network using Uniprobe and JASPAR. Protein phosphorylations were examined by phosphoprotein/peptide enrichment, followed by mass spectrometry analysis. Phosphorylations were compared to Phospho.ELM, and PhosphoSite. The metabolome mapping was established using KEGG and BIGG databases.

3. Results

To understand how mitochondria regulate their morphology and function, we first analyzed mitochondrial morphology quantitatively in ARPE-19 cells subjected to oxidative stress conditions using a systematic computational model (**Figure 1**). Representative mitochondrial images at selected time points (0.5, 1, 8, 24 h) are shown for clear comparison **Figure 1**). We examined mitochondrial area, circularity, perimeter, content as well as cellular area to identify changes between healthy and injured mitochondria. Previously, our *in vitro* data using RPE cells demonstrated the positive correlation between apoptotic signaling and mitochondria-nucleus prohibitin shuttling. Our previous studies suggest that cellular distribution and the total volume of mitochondria could be affected by microtubules, intermediate filaments and cardiolipin [24–27, 29, 30].

http://dx.doi.org/10.5772/intechopen.75994

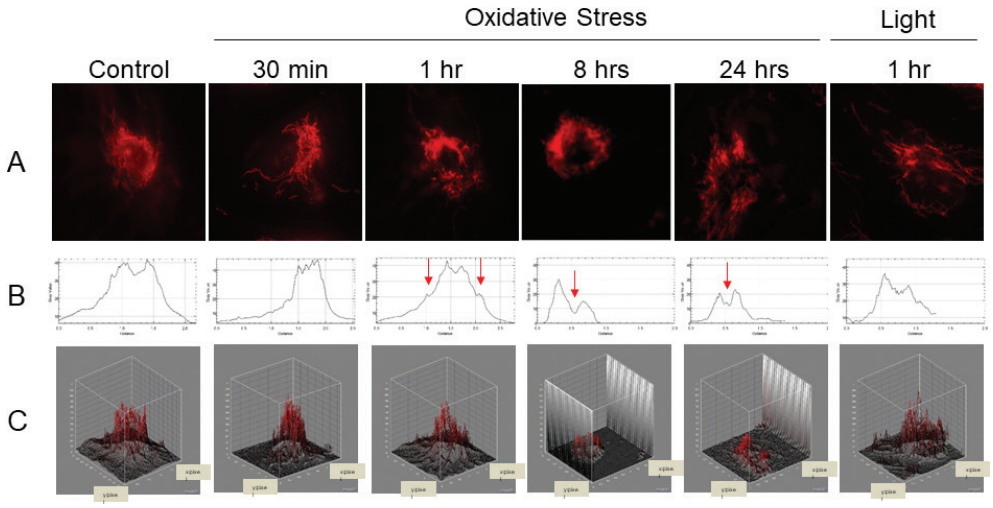

Figure 1. Quantitative analysis of mitochondrial morphology: representative images of MitoTracker Orange-labeled mitochondria from ARPE-19 cells exposed to *t*-BuOOH for 0.5–24 h or light for 1 h are shown here. A. ARPE-19 cells under oxidative stress were analyzed by immunocytochemistry using MitoTracker. B. Mitochondrial content was represented by 2D graph (radius/intensity) showing decreased size and fragmentation pattern under stress conditions. C. Mitochondria in ARPE-19 cells were presented in 3D structure using Image J software.

Our results showed that the connectivity, the number of mitochondrial branch points, and the interactive isosurfaces were altered at the contact sites between mitochondria and other organelles. Under extended oxidative stress (1, 8, 24 h) and intense light (7000 lx, 1 h), we observed a decrease in mitochondrial size, presence of fragmented filaments (red arrows), and holes on the organelle contact sites. Under intense light condition, mitochondria in ARPE-19 cells were decreased and fragmented as shown in oxidative stress (1–8 h).

Next, mitochondrial perimeter vs. circularity was examined to determine the correlation between mitochondrial morphology and oxidative stress (**Figure 2**). We hypothesized that some mitochondrial indexes that include circularity and perimeter ratio may represent mitochondrial dynamics. We calculated mitochondrial area, perimeter, minor axis, and circularity to conclude that specific mitochondrial ratio correlated positively with stress kinetics.

The average mitochondrial area/perimeter ratio normalized to the minor axis suggests that specific conditions may induce mitochondrial swelling (**Figure 3**). Time-dependent decrease of minor axis and mitochondrial area/perimeter normalized to the circularity was noticed under stress condition. Our previous proteomic study demonstrated that tubulin/vimentin depolymerization and phosphorylations increased in stressed mitochondria [25].

To understand mitochondrial dynamics in detail, mitochondrial trafficking complex was examined. Subcellular fractionation, immunoprecipitation using primary prohibitin antibody, native gel, and mass spectrometry analysis suggest that motor protein complex may determine mitochondrial dynamics and retrograde signaling under stress conditions. Molecular motor

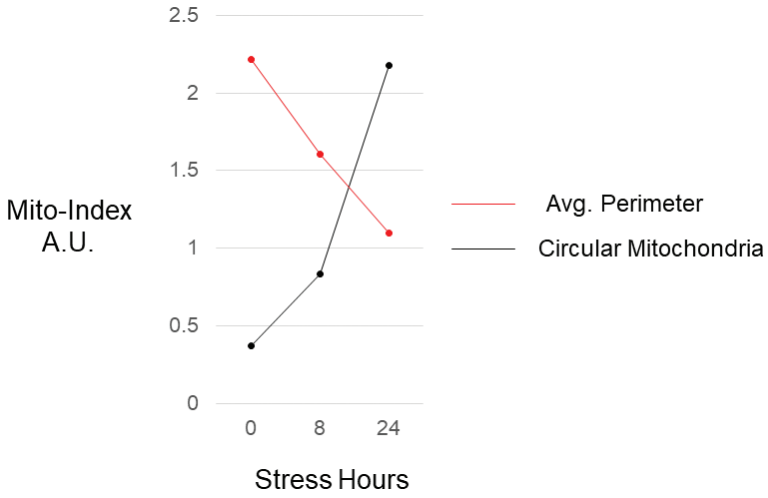

Figure 2. Quantitative analysis of mitochondrial morphology: perimeter vs. circularity. X axis represents time of ARPE-19 cells under oxidative stress and Y axis represents mitochondrial index on perimeter vs. circularity ratio in arbitrary units. Selected time points are 0, 8, 24 h were shown for clarity [24]. Our calculation demonstrated that mitochondria under oxidative stress change their morphology to circular shape for fusion, followed by fragmentation toward greater degree of roundness and circularity. Total area of mitochondria decreased to 40–50% and both perimeter/circular mitochondria were downregulated to 60–70%. Area/perimeter normalized to circularity ratio of mitochondria was decreased to 63% (1 h oxidative stress), showing a positive correlation between mitochondrial morphology changes and apoptotic RPE.

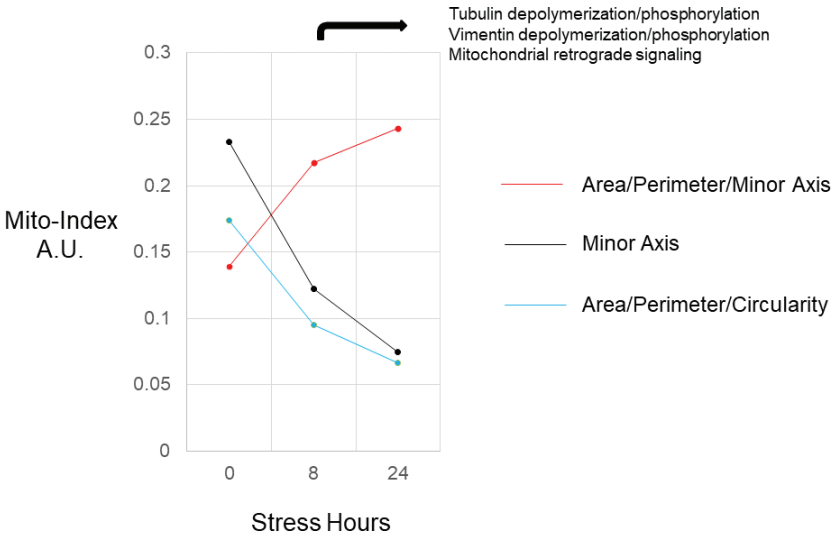

Figure 3. Mitochondrial index: mitochondrial area/perimeter/minor axis vs. minor axis vs. area/perimeter/circularity. X axis represents stressed time (hrs) of ARPE-19 under oxidants and Y axis represents mitochondrial index showing mitochondrial area/perimeter/minor axis (red), compared to mitochondrial minor axis (black), and mitochondrial area/perimeter/mitochondrial circularity (blue) in arbitrary units.

complex contains plus-end-directed kinesin 19, myosin 9, protocadherin gA7, and prohibitin (**Figure 4**). The molecular motor/adaptor/receptor complex mediates mitochondrial dynamics. Motor proteins, including kinesin and myosin, facilitate mitochondrial trafficking along the cytoskeleton, mainly microtubules, actin polymers and intermediate filaments (**Figure 5**). Domain analysis of mitochondrial trafficking complex showed that plus-end-directed kinesin 19 (ATP and Mg^{2+} binding domains), myosin 9 (myosin head motor domain, SH3 domain, ATP binding domain), protocadherin gA7 (cadherin repeat and Ca^{2+} binding domain), and prohibitin (PX domain, lipid binding pocket) exist in the trafficking complex.

In order to correlate our *in vitro* findings with human pathology, we analyzed mitochondrial trafficking complex in human postmortem AMD eyes using a proteomic approach (**Figure 6**). RPE and retina tissues (central vs. peripheral) from AMD eyes and age-matching control eyes were analyzed by phosphoproteomics and mass spectrometry analysis. We observed different expression levels of prohibitin, inositol receptor, calponin, ankyrin, guanylate cyclase, and NADP ubiquinone oxidoreductase in the RPE and pyruvate kinase, PP2A, creatine kinase, PAK S/T kinase, vimentin, FES tyrosine kinase and dynamin like protein in the retina from AMD samples compared to control. Our results suggest that mitochondrial trafficking could be a significant determinant of RPE apoptosis by decreased prohibitin. Further, Ca^{2+}, Fe^{2+}, inositide, phosphorylation, and energy imbalance may lead to the accelerated pathogenesis toward AMD.

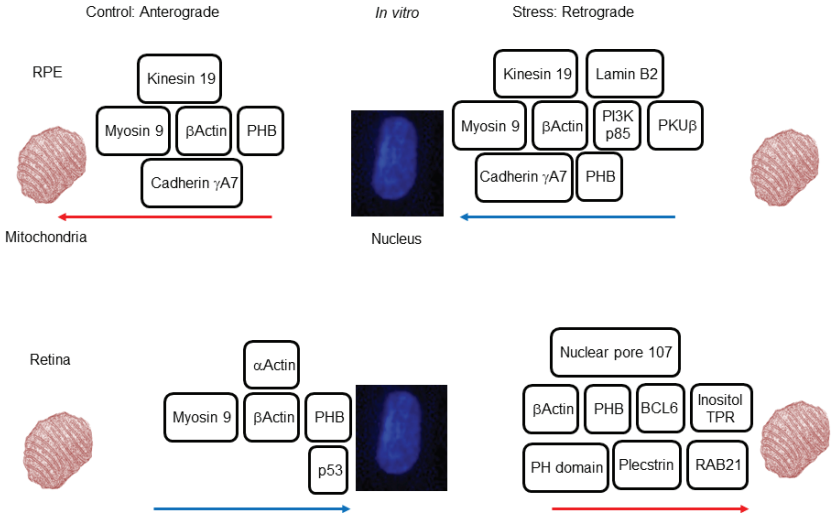

Figure 4. Mitochondrial Trafficking Complex *in vitro*: Retrograde vs. Anterograde Signal. Protein complex in ARPE-19 (RPE) and HRP (retina) cells were analyzed using immunoprecipitation and mass spectrometry. Under normal condition, trafficking complex including prohibitin translocalizes into mitochondria (anterograde) whereas trafficking complex moves into the nucleus (retrograde) under oxidative stress in RPE cells. The molecular motor/adaptor/receptor complex mediates mitochondrial anterograde vs. retrograde signaling. However, in the retina, retrograde signal (mitochondria to the nucleus) is dominant under normal condition, probably due to increased p53 signaling (prohibitin found in the nucleus).

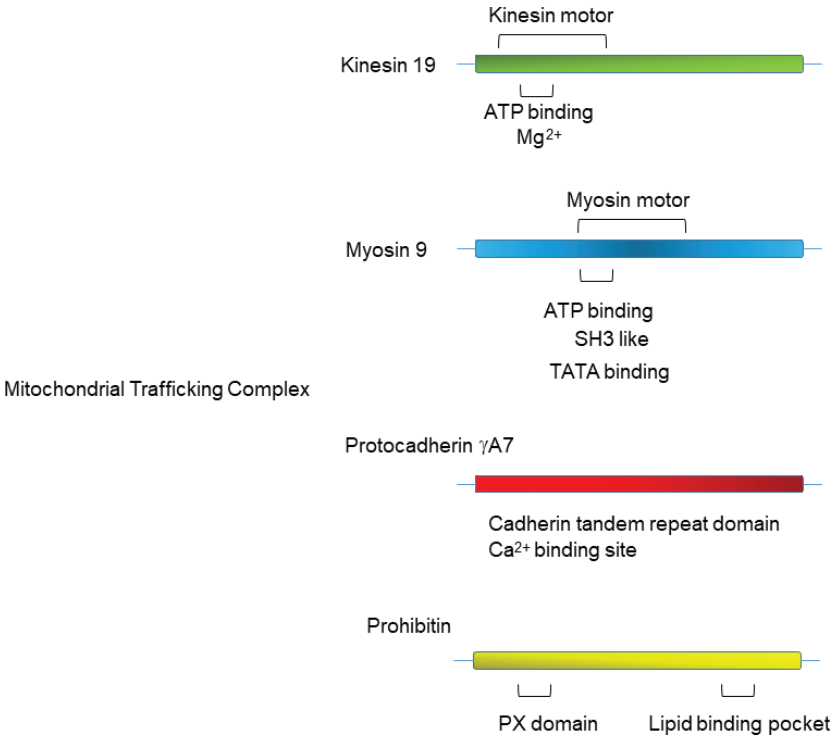

Figure 5. Domain analysis of mitochondrial trafficking complex: ATP, Ca^{2+}, and lipid-dependent signaling. Prohibitin binding proteins were analyzed using bioinformatics software and databases, including iHOP, InterPro (https://www.ebi.ac.uk/interpro/), Expasy/Prosite (https://prosite.expasy.org/), conserved domain search (https://www.ncbi.nlm.nih.gov/Structure/cdd/wrpsb.cgi), Motif (https://molbiol-tools.ca/Motifs.htm) and Pfam (http://pfam.xfam.org/). Kinesin 19 contains ATP binding domain and kinesin motor domain, whereas Myosin 9 has SH3, ATP binding, TATA binding, and myosin motor domains. Protocadherin γA7 includes repeat domain and calcium binding sequences. Prohibitin contains PX domain and the second lipid binding domain.

It is proposed that specific organelles, including mitochondria, melanosome, and phagosome, may use different kinesin and myosin motors for their distribution and trafficking in the RPE [25, 31–33]. Mitochondrial trafficking could be determined by ATP, Ca^{2+}, and lipid interactions based on their domain analysis [29, 34–38] and mitochondrial trafficking is a significant determinant of RPE apoptosis [24, 37]. Altered concentrations of mitochondrial complex, phosphoproteins, and ATP/ADP may lead to premature senescence in RPE cells [27]. Our enriched phosphoproteins and phosphopeptides analysis demonstrated that altered inositol triphosphate receptor, ankyrin, NADP reactions exist in AMD (**Figure 6**). Regulation of mitochondrial complex/lipid ratio and the energy producing machinery may enable enhanced longevity of RPE cells.

Next, a 3D surface model was used to analyze mitochondrial nodes, edges, branches, and tubular filaments (**Figure 7**). Cellular distribution and the total volume were affected by microtubules, intermediate filaments and cardiolipin. A 3D model showed that mitochondrial contact sites with endoplasmic reticulum (ER) and/or the nucleus were opened irreversibly under extended stress (24 h).

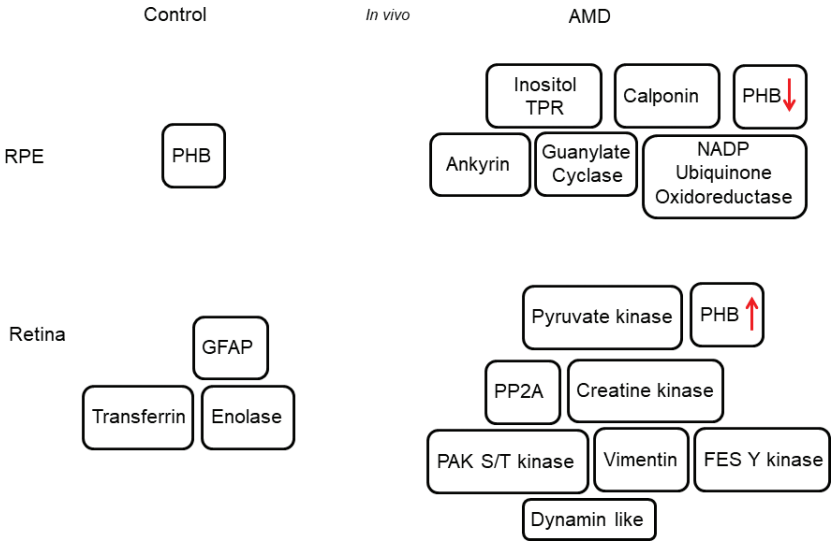

Figure 6. Mitochondrial signaling in the retina and RPE *in vivo* using human AMD eyes: mitochondrial trafficking is a significant determinant of RPE apoptosis. RPE and retina tissues (central vs. peripheral) from AMD eyes and age-matching control eyes were analyzed using phosphoproteomics and mass spectrometry analysis. We observed different expressions of inositol receptor, calponin, ankyrin, guanylate cyclase, and NADP ubiquinone oxidoreductase in the RPE and pyruvate kinase, PP2A, creatine kinase, PAK S/T kinase, vimentin, FES tyrosine kinase and dynamin like protein in the retina from AMD samples compared to control. Altered concentrations of mitochondrial complex, phosphoproteins, and ATP/ADP may lead to premature senescence in RPE cells.

In order to understand AMD protein network, the new AMD interactome with oxidative biomarkers was established using phosphoproteomics data and a computational model. The current AMD interactome demonstrated that several earlier unrelated to AMD proteins, including ubiquitin, peroxiredoxin, MAP kinase, BUB 1/3, vimentin and crystalline could be involved in AMD progression, suggesting that cytoskeletal protein phosphorylation, crystalline aggregation, and mitochondrial signaling may contribute to RPE apoptosis (**Figure 8**). To confirm oxidative stress biomarkers, specific cytoskeletal protein changes were determined *in vivo* using animal model previously (C3H female mice, 7 weeks old) [25, 30, 38]. Neurofilament, vimentin, and tubulin were upregulated under 24 h constant light compared to 12 h dark/12 h light condition [38].

3.1. Discussion

The current study determined the mitochondrial morphology quantitatively using a mathematic model and mitochondrial trafficking complex under stress conditions. Our data suggest that the kinesin-myosin-cadherin-prohibitin complex could be involved in anterograde mitochondrial trafficking, whereas PKUb S/T kinase-myosin-PI3K-lamin B2 bindings may regulate an energy demanding retrograde transport of mitochondria [25, 39–43]. Prohibitin binding with a trafficking protein complex may regulate the bidirectional transport of mitochondria along actin microfilaments, intermediate filaments, and microtubules. The mitochondrial trafficking complex implies that a specific mechanism of communication may exist in the ATP

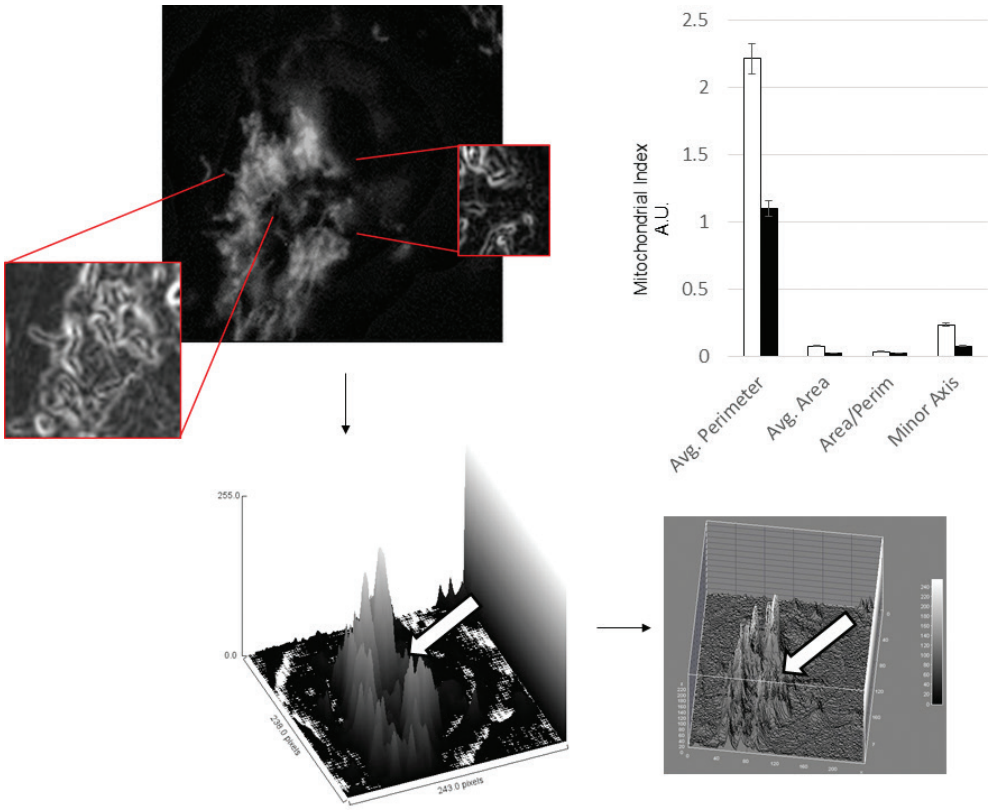

Figure 7. A 3D surface model and a graph representation by nodes, edges, branches, and tubular filaments: Mitochondrial filaments in three dimensions in RPE cells were calculated quantitatively. The connectivity, the number of mitochondrial branch points, and the interactive 3D visualization of isosurfaces were examined to identify the contact point between mitochondria and other organelles, including ER and the nucleus (white arrow). Mitochondria under oxidative stress (24 hrs) decreased their average perimeter (49%), average area (28%), area/perimeter (56%), and minor axis (32%).

and Ca^{2+} demanding regions. Mitochondrial dysfunction, altered dynamics, impaired transport, and turnover perturbation are associated with AMD.

Oxidative stress-induced apoptosis is the final cell death pathway in many irreversible ocular diseases that include AMD. While the end point of apoptosis is well established, the knowledge of early biochemical reactions and specific molecular players has been elusive. We have examined early biosignatures and mechanisms of retinal and RPE cell death under oxidative stress [44]. Our previous studies demonstrated that not only intense light but also constant moderate light and mild oxidative stress may trigger induction of anti-apoptotic Bcl-xL and erythropoietin (EPO) as well as pro-apoptotic caspases [24, 25, 27–29, 37, 38, 45–47]. We determined that protein modifications, including nitration and phosphorylation, were altered under oxidative stress possibly due to excess of NO production [26, 48–50].

The analysis of AMD interactome using proteome-genome-metabolome network suggests that there is a positive correlation between mitochondrial retrograde signaling and AMD progression. The AMD interactome suggests: (1) network-based interactions among AMD-related

http://dx.doi.org/10.5772/intechopen.75994

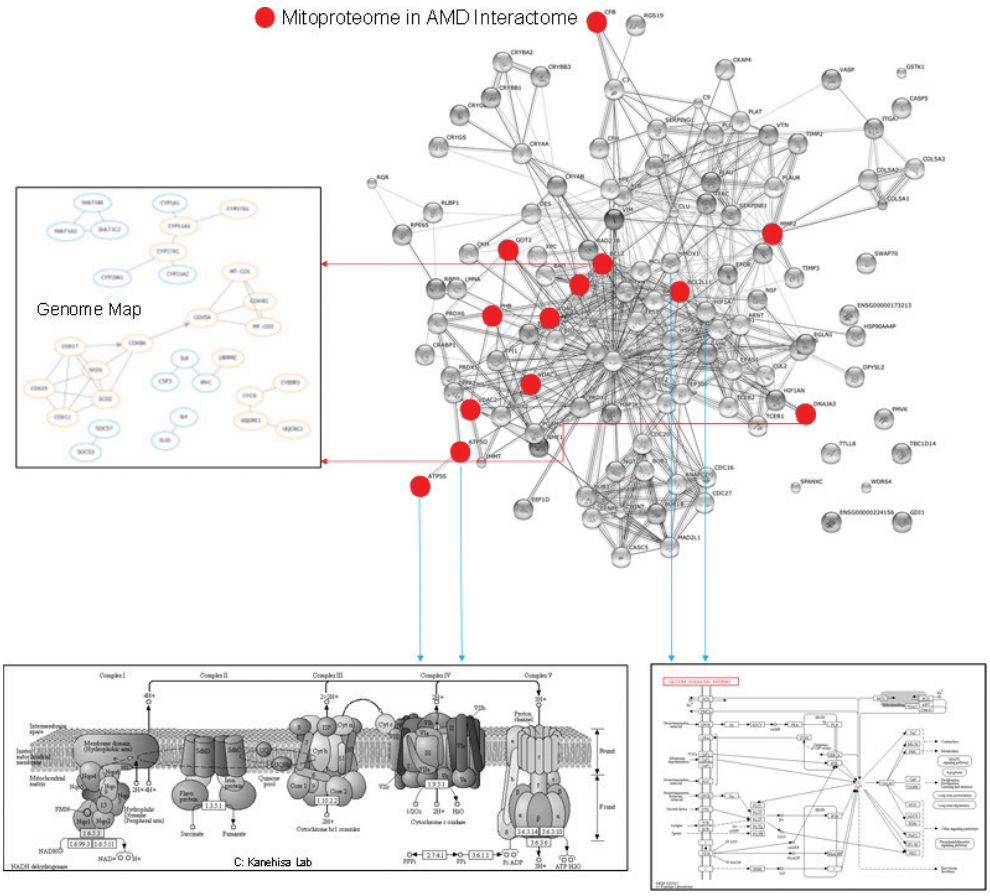

Figure 8. Genome-proteome-metabolome mapping in AMD: retrograde mitochondrial signaling. The protein interactome was established using STRING software and our proteomics data. The genome regulatory network was connected to the proteome network using Uniprobe and JASPAR. Protein phosphorylations were examined by phosphoprotein/peptide enrichment, followed by mass spectrometry analysis. Phosphorylations were compared to Phospho.ELM, and PhosphoSite. The metabolome mapping was established using KEGG and BIGG databases. Based on our proteomics and the interactome data that identified altered signaling of apoptosis in the retina and RPE both *in vitro and in vivo*, the pathological pathway determined by the AMD interactome could yield suitable targets for anti-apoptotic and anti-angiogenic therapy: (1) mitochondrial dysfunction in the peripheral RPE (prohibitin, ATP synthase); (2) oxidative stress including intense and constant light (peroxiredoxin, thioredoxin, glutathione S-transferase); (3) cytoskeletal remodeling by microtubule, actin filament, and intermediate filament (vimentin, actin, tubulin); (4) high concentration of nitric oxide (nitric oxide synthase), (5) hypoxia (HIF1, erythropoietin, VEGF); (6) disrupted circadian clock (melatonin); (7) apoptotic downstream (pJAK2, pSTAT3, Bclxl, caspases); (8) altered lipid concentrations (cardiolipin, cholesterol); (9) altered visual cycle (CRABP, CRALBP, RPE65); (10) altered energy metabolism (S/T vs. Y kinases, carnitine, pyruvate, ATP synthase); (11) aggregation of heat shock proteins and crystallins; and (12) inflammation (CFH, C3, collagen, vitronectin).

hub proteins that include UBC, MMP2, BCL, PRDX, ATP5O, C3, TF, and CRYAB, (2) increased local interactions between oxidative stress, complement activation, transcription, metabolism, (3) AMD module as a cluster in the same network neighborhood, (4) potential causal molecules including Ca^{2+}, Fe^{2+}, ATP/ADP, OPO_4^{2-}, lipids, (5) altered cytoskeleton, microtubule, abnormal mitochondrial signaling.

The mitochondrial interactome provides a base for better understanding of oxidative stress-induced apoptosis and the mechanism of age-related diseases, including AMD. As a consequence, an effective treatment of neurodegenerative diseases based on the modulation of mitochondrial network is expected to result.

Author details

Srinivas R. Sripathi[1], Weilue He[2], Johnpaul Offor[3], Diana R. Gutsaeva[4] and Wan Jin Jahng[5]*

*Address all correspondence to: wan.jahng@aun.edu.ng

1 Department of Ophthalmology, Wilmer Eye Institute, The Johns Hopkins University School of Medicine, Baltimore, USA

2 Department of Biomedical Engineering, Michigan Technological University, Houghton, USA

3 Department of Natural and Environmental Sciences, American University of Nigeria, Yola, Nigeria

4 Department of Ophthalmology, Augusta University, Augusta, USA

5 Retina Proteomics Laboratory, Department of Petroleum Chemistry, American University of Nigeria, Yola, Nigeria

References

[1] Chen H, Chan DC. Mitochondrial dynamics in mammals. Current Topics in Developmental Biology. 2004;**59**:119-144. DOI: 10.1016/S0070-2153(04)59005-1

[2] Castegna A, Iacobazzi V, Infantino V. The mitochondrial side of epigenetics. Physiological Genomics. 2015;**47**:299-307. DOI: 10.1152/physiolgenomics.00096.2014

[3] Hailey DW, Rambold AS, Satpute-Krishnan P, Mitra K, Sougrat R, Kim PK, Lippincott-Schwartz J. Mitochondria supply membranes for autophagosome biogenesis during starvation. Cell. 2010;**141**:656-667. DOI: 10.1016/j.cell.2010.04.009

[4] Chen H, McCaffery JM, Chan DC. Mitochondrial fusion protects against neurodegeneration in the cerebellum. Cell. 2007;**130**:548-562. DOI: 10.1016/j.cell.2007.06.026

[5] Gomes LC, Di Benedetto G, Scorrano L. During autophagy mitochondria elongate, are spared from degradation and sustain cell viability. Nature Cell Biology. 2011;**13**:589-598. DOI: 10.1038/ncb2220

[6] Gerhold JM, Cansiz-Arda Ş, Lõhmus M, Engberg O, Reyes A, Rennes H Van, Sanz A, Holt IJ, Cooper HM, Spelbrink JN. Human mitochondrial DNA-protein complexes attach to a cholesterol- rich membrane structure. Scientific Reports. 2015;**5**:1-14. DOI: 10.1038/srep15292

[7] Schrier SA, Falk MJ. Mitochondrial disorders and the eye. Current Opinion in Ophthalmology. 2011;**22**:325-331. DOI: 10.1097/ICU.0b013e328349419d

[8] Mikhed Y, Daiber A, Steven S. Mitochondrial oxidative stress, mitochondrial DNA damage and their role in age-related vascular dysfunction. International Journal of Molecular Sciences. 2015;**16**:15918-15953. DOI: 10.3390/ijms160715918

[9] Liang P, MacRae TH. Molecular chaperones and the cytoskeleton. Journal of Cell Science. 1997;**110**(Pt 1):1431-1440

[10] Rambold AS, Kostelecky B, Elia N, Lippincott-Schwartz J. Tubular network formation protects mitochondria from autophagosomal degradation during nutrient starvation. Proceedings of the National Academy of Sciences of the United States of America. 2011;**108**:10190-10195. DOI: 10.1073/pnas.1107402108

[11] Vilalta PM, Zhang L, Hamm-Alvarez SF. A novel taxol-induced vimentin phosphorylation and stabilization revealed by studies on stable microtubules and vimentin intermediate filaments. Journal of Cell Science. 1998;**111**(Pt 1):1841-1852 Available from: http://www.ncbi.nlm.nih.gov/pubmed/9625747

[12] Legros F, Malka F, Frachon P, Lombès A, Rojo M. Organization and dynamics of human mitochondrial DNA. Journal of Cell Science. 2004;**117**:2653-2662. DOI: 10.1242/jcs.01134

[13] Hoye AT, Davoren JE, Wipf P, Fink MP, Kagan VE. Targeting mitochondria. Accounts of Chemical Research. 2008;**41**:87-97. DOI: 10.1021/ar700135m

[14] Dai Z, Yin J, He H, Li W, Hou C, Qian X, Mao N, Pan L. Mitochondrial comparative proteomics of human ovarian cancer cells and their platinum-resistant sublines. Proteomics. 2010;**10**:3789-3799. DOI: 10.1002/pmic.200900685

[15] Lee J, Giordano S, Zhang J. Autophagy, mitochondria and oxidative stress: Cross-talk and redox signalling. The Biochemical Journal. 2012;**441**:523-540. DOI: 10.1042/bj20111451

[16] Terluk MR, Kapphahn RJ, Soukup LM, Gong H, Gallardo C, Montezuma SR, Ferrington DA. Investigating mitochondria as a target for treating age-related macular degeneration. The Journal of Neuroscience. 2015;**35**:7304-7311. DOI: 10.1523/JNEUROSCI.0190-15.2015

[17] Feher J, Kovacs I, Artico M, Cavallotti C, Papale A, Balacco Gabrieli C. Mitochondrial alterations of retinal pigment epithelium in age-related macular degeneration. Neurobiology of Aging. 2006;**27**:983-993. DOI: 10.1016/j.neurobiolaging.2005.05.012

[18] Suter M, Remé C, Grimm C, Wenzel A, Jäättela M, Esser P, Kociok N, Leist M, Richter C. Age-related macular degeneration: The lipofuscin component N-retinyl-N-retinylidene ethanolamine detaches proapoptotic proteins from mitochondria and induces apoptosis in mammalian retinal pigment epithelial cells. The Journal of Biological Chemistry. 2000;**275**:39625-39630. DOI: 10.1074/jbc.M007049200

[19] Beal MF. Mitochondria take center stage in aging and neurodegeneration. Annals of Neurology. 2005;**58**:495-505. DOI: 10.1002/ana.20624

[20] Liu Z, Butow RA. Mitochondrial retrograde signaling. Annual Review of Genetics. 2006;**40**:159-185. DOI: 10.1146/annurev.genet.40.110405.090613

[21] Brown K, Liu Y, Chen D. Aging: The mitochondrial connection. Journal of Clinical and Experimental Pathology. 2012;**S4**:003. DOI: 10.4172/2161-0681.S4-003

[22] Ambati J, Anand A, Fernandez S, Sakurai E, Lynn BC, Kuziel WA, Rollins BJ, Ambati BK. An animal model of age-related macular degeneration in senescent Ccl-2- or Ccr-2-deficient mice. Nature Medicine. 2003;**9**:1390-1397. DOI: 10.1038/nm950

[23] Kenney MC, Atilano SR, Boyer D, Chwa M, Chak G, Chinichian S, Coskun P, Wallace DC, Nesburn AB, Udar NS. Characterization of retinal and blood mitochondrial DNA from age-related macular degeneration patients. Investigative Ophthalmology and Visual Science. 2010;**51**:4289-4297. DOI: 10.1167/iovs.09-4778

[24] Sripathi SR, He W, Atkinson CL, Smith JJ, Liu Z, Elledge BM, Jahng WJ. Mitochondrial-nuclear communication by prohibitin shuttling under oxidative stress. Biochemistry. 2011;**50**:8342-8351. DOI: 10.1021/bi2008933

[25] Sripathi SR, He W, Sylvester O, Neksumi M, Um J-Y, Dluya T, Bernstein PS, Jahng WJ. Altered cytoskeleton as a mitochondrial decay signature in the retinal pigment epithelium. The Protein Journal. 2016;**35**:179-192. DOI: 10.1007/s10930-016-9659-9

[26] Sripathi SR, He W, Um J, Moser T, Dehnbostel S, Kindt K, Goldman J, Frost MC, Jahng WJ. Nitric oxide leads to cytoskeletal reorganization in the retinal pigment epithelium under oxidative stress. Advances in Bioscience and Biotechnology. 2012;**03**:1167-1178. DOI: 10.4236/abb.2012.38143

[27] Sripathi S, He W, Prigge CL, Sylvester O, Um J-Y, Powell FL, Neksumi M, Bernstein PS, Choo D-W, Bartoli M, Gutsaeva DR, Jahng WJ. Interactome mapping guided by tissue-specific phosphorylation in age-related macular degeneration. International Journal of Scientific and Engineering Research. 2017;**8**:680-698. DOI: 10.14299/ijser.2017.02.010

[28] Lee H, Chung H, Lee SH, Jahng WJ. Light-induced phosphorylation of crystallins in the retinal pigment epithelium. International Journal of Biological Macromolecules. 2011;**48**:194-201. DOI: 10.1016/j.ijbiomac.2010.11.006

[29] Sripathi SR, Sylvester O, He W, Moser T, Um J-Y, Lamoke F, Ramakrishna W, Bernstein PS, Bartoli M, Jahng WJ. Prohibitin as the molecular binding switch in the retinal pigment epithelium. The Protein Journal. 2016;**35**:1-16. DOI: 10.1007/s10930-015-9641-y

[30] Sripathi SR, Prigge CL, Elledge B, He W, Offor J, Gutsaeva DR, Jahng WJ. Melatonin modulates prohibitin and cytoskeleton in the retinal pigment epithelium. International Journal of Scientific & Engineering Research. 2017;**8**:502-506

[31] Brickley K, Stephenson FA. Trafficking kinesin protein (TRAK)-mediated transport of mitochondria in axons of hippocampal neurons. The Journal of Biological Chemistry. 2011;**286**:18079-18092. DOI: 10.1074/jbc.M111.236018

[32] Williams DS. Transport to the photoreceptor outer segment by myosin VIIa and kinesin II. Vision Research. 2002;**42**:455-462. DOI: 10.1016/S0042-6989(01)00228-0

[33] Miki H, Setou M, Kaneshiro K, Hirokawa N. All kinesin superfamily protein, KIF, genes in mouse and human. Proceedings of the National Academy of Sciences of the United States of America. 2001;**98**:7004-7011. DOI: 10.1073/pnas.111145398

[34] Huang H, Frohman MA. Lipid signaling on the mitochondrial surface. Biochimica et Biophysica Acta, Molecular and Cell Biology of Lipids. 2009;**1791**:839-844. DOI: 10.1016/j.bbalip.2009.05.012

[35] MacAskill AF, Rinholm JE, Twelvetrees AE, Arancibia-Carcamo IL, Muir J, Fransson A, Aspenstrom P, Attwell D, Kittler JT. Miro1 is a calcium sensor for glutamate receptor-dependent localization of mitochondria at synapses. Neuron. 2009;**61**:541-555. DOI: 10.1016/j.neuron.2009.01.030

[36] Fransson Å, Ruusala A, Aspenström P. The atypical Rho GTPases Miro-1 and Miro-2 have essential roles in mitochondrial trafficking. Biochemical and Biophysical Research Communications. 2006;**344**:500-510. DOI: 10.1016/j.bbrc.2006.03.163

[37] Lee H, Arnouk H, Sripathi S, Chen P, Zhang R, Bartoli M, Hunt RC, Hrushesky WJM, Chung H, Lee SH, Jahng WJ. Prohibitin as an oxidative stress biomarker in the eye. International Journal of Biological Macromolecules. 2010;**47**:685-690. DOI: 10.1016/j.ijbiomac.2010.08.018

[38] Zhang R, Hrushesky WJM, Wood PA, Lee SH, Hunt RC, Jahng WJ. Melatonin reprogrammes proteomic profile in light-exposed retina in vivo. International Journal of Biological Macromolecules. 2010;**47**:255-260. DOI: 10.1016/j.ijbiomac.2010.04.013

[39] Mishra S, Ande SR, Nyomba BLGG. The role of prohibitin in cell signaling. The FEBS Journal. 2010;**277**:3937-3946. DOI: 10.1111/j.1742-4658.2010.07809.x

[40] Rudel T, Kepp O, Kozjak-Pavlovic V, Santhanam S, Venkatraman A, Ramakrishna BS, Tirosh O, Levy EE, Reifen R, Damiani CR, Benetton CAF, Stoffel C, Bardini KC, Cardoso VH, Di Giunta G, Pinho RA, Dal-Pizzol F, Streck EL, Restivo NL, Srivastava MD, Schafer IA, Hoppel CL, Sifroni KG, Damiani CR, Stoffel C, Cardoso MR, Ferreira GK, Jeremias IC, Rezin GT, Scaini G, Schuck PF, Dal-Pizzol F, Streck EL, D'Argenio G, Calvani M, Casamassimi A, Petillo O, Margarucci S, Rienzo M, Peluso I, Calvani R, Ciccodicola A, Caporaso N, Peluso G, Baregamian N, Song J, Bailey CE, Papaconstantinou J, Evers BM, Chung DH, Briet F, Twomey C, Jeejeebhoy KN, Demine S, Reddy N, Renard P, Raes M, Arnould T, Farhadi A, Keshavarzian A, Van De Kar LD, Jakate S, Domm A, Zhang L, Shaikh M, Banan A, Fields JZ, He D, Sougioultzis S, Hagen S, Liu J, Keates S, Keates AC, Pothoulakis C, Lamont JT, Hsieh S-Y, Shih TC, Yeh C-Y, Lin C-J, Chou Y-Y, Lee Y-S, Kamizato M, Nishida K, Masuda K, Takeo K, Yamamoto Y, Kawai T, Teshima-Kondo S, Tanahashi T, Rokutan K, Kuwano Y, Tominaga K, Kawahara T, Sasaki H, Takeo K, Nishida K, Masuda K, Kawai T, Teshima-Kondo S, Rokutan K, Montgomery MK, Turner N, Nazli A, Yang P-C, Jury J, Howe K, Watson JL, Söderholm JD, Sherman PM, Perdue MH, McKay DM, Schürmann G, Brüwer M, Klotz A, Schmid KW, Senninger N, Zimmer K-P, Vanderborght M, Nassogne MC, Hermans D, Moniotte S, Seneca S, Van Coster R, Buts JP, Sokal EM, Manuscript A, Rath E, Haller D, Han J, Yu C, Souza RF, Theiss AL, Dehghan F, Lz A, Karimian H, Yahayu M, Gc E, As F, H MA, Taha R, Seidman E, Mailhot G, Boudreau F, Gendron FP, Beaulieu JF, Ménard D, Delvin E, Amre D, Levy EE, Mayall TP, Bjarnason I, Khoo UY, Peters TJ, Macpherson AJ. Mitochondrial dysfunction and insulin resistance: An update. Journal of Pediatric Gastroenterology and Nutrition. 2014;**4**:1172-1184. DOI: 10.1007/s00535-009-0119-6

[41] Schleicher M, Shepherd BR, Suarez Y, Fernandez-Hernando C, Yu J, Pan Y, Acevedo LM, Shadel GS, Sessa WC. Prohibitin-1 maintains the angiogenic capacity of endothelial cells by regulating mitochondrial function and senescence. The Journal of Cell Biology. 2008;**180**:101-112. DOI: 10.1083/jcb.200706072

[42] Peng Y-TT, Chen P, Ouyang R-YY, Song L. Multifaceted role of prohibitin in cell survival and apoptosis. Apoptosis. 2015;**20**:1135-1149. DOI: 10.1007/s10495-015-1143-z

[43] Jiang L, Dong P, Zhang Z, Li C, Li Y, Liao Y, Li X, Wu Z, Guo S, Mai S, Xie D, Liu Z, Zhou F. Akt phosphorylates prohibitin 1 to mediate its mitochondrial localization and promote proliferation of bladder cancer cells. Cell Death & Disease. 2015;**6**:e1660. DOI: 10.1038/cddis.2015.40

[44] Jahng WJ. New biomarkers in the retina and RPE under oxidative stress. In: Adio A, editor. Ocular Diseases. InTech; 2012. DOI: 10.5772/48785

[45] Lee H, Chung H, Arnouk H, Lamoke F, Hunt RC, Hrushesky WJM, Wood PA, Lee SH, Jahng WJ. Cleavage of the retinal pigment epithelium-specific protein RPE65 under oxidative stress. International Journal of Biological Macromolecules. 2010;**47**:104-108. DOI: 10.1016/j.ijbiomac.2010.05.014

[46] Arnouk H, Lee H, Zhang R, Chung H, Hunt RC, Jahng WJ. Early biosignature of oxidative stress in the retinal pigment epithelium. Journal of Proteomics. 2011;**74**:254-261. DOI: 10.1016/j.jprot.2010.11.004

[47] Sripathi SR, He W, Um JY, Moser T. Nitric oxide leads to cytoskeletal reorganization in the retinal pigment epithelium under oxidative stress. Advances in Bioscience and Biotechnology. 2012;**03**:1167-1178. DOI: 10.4236/abb.2012.38143

[48] Lopez CJ, Qayyum I, Mishra OP, Delivoria-Papadopoulos M. Effect of nitration on protein tyrosine phosphatase and protein phosphatase activity in neuronal cell membranes of newborn piglets. Neuroscience Letters. 2005;**386**:78-81. DOI: 10.1016/j.neulet.2005.04.089

[49] Rayala SK, Martin E, Sharina IG, Molli PR, Wang X, Jacobson R, Murad F, Kumar R. Dynamic interplay between nitration and phosphorylation of tubulin cofactor B in the control of microtubule dynamics. Proceedings of the National Academy of Sciences of the United States of America. 2007;**104**:19470-19475. DOI: 10.1073/pnas.0705149104

[50] Di Stasi AM, Mallozzi C, Macchia G, Petrucci TC, Minetti M. Peroxynitrite induces tryosine nitration and modulates tyrosine phosphorylation of synaptic proteins. Journal of Neurochemistry. 1999;**73**:727-735 Available from: http://www.ncbi.nlm.nih.gov/pubmed/10428070